Assessment of the wall shear stress measurement with arrayed micro hot-film sensors in a turbulent channel flow

Takashi Yoshino, Yuji Suzuki, Nobuhide Kasagi

Department of Mechanical Engineering,
The University of Tokyo
Hongo, Bunkyo-ku, Tokyo 113-8656, Japan
yoshino@thtlab.t.u-tokyo.ac.jp

Shoji Kamiunten

Research & Development Headquarters,
Yamatake Corporation
Kawana, Fujisawa, Kanagawa 251-8522, Japan

ABSTRACT

Arrayed micro hot-film sensors for the measurement of the streamwise and spanwise wall shear stresses were developed and evaluated in a turbulent channel flow. The bandwidth of the sensor is found to be much narrower than previous estimates in the literature. A numerical analysis of the unsteady thermal field around the sensor chip is made in order to obtain a clue to design a hot-film shear stress sensor having higher frequency response. It is found that the phase lag of the thermal boundary layer above the hot-film and the indirect convective heat transfer through the diaphragm are responsible for the deteriorated sensor response.

INTRODUCTION

In the last decade, feedback control of wall turbulence attracts much attention because of its potential of high control performance with a small energy input (e.g., Moin & Bewley, 1994; Gad-el-Hak, 1996; Kasagi, 1998). In this control mode, the near-wall coherent structures, which are responsible for the turbulent transport mechanism, should be detected by sensors mounted on the wall. Wall shear stress sensors are considered to be one of the most feasible candidates to achieve this goal.

Recent development of microelectromechanical systems (MEMS) technology makes it possible to fabricate a mechanical device having submillimeter scale. For the measurement of wall shear stress fluctuation, various sensors are proposed, such as an electrochemical sensor (Mitchell & Hanratty, 1966), a micro floating element (Schmidt et al., 1988) and an optical sensor using fan fringes of laser light (Naqwi & Reynolds, 1991; Obi et al., 1996). In the present study, a thermal sensor is adopted because its microfabrication process is relatively simple. Alfredsson et al. (1988) claimed that the frequency response of the hot-film sensors is deteriorated due to the heat conduction loss to the substrate. Jiang et al. (1996) developed an array of micro hot-film shear stress sensors and demonstrated that the shear stress distribution was measured with high spatial resolution. They also reported that the frequency response of their sensors is much improved by reducing the heat conduction to the substrate with an insulating vacuum cavity, and they estimated the bandwidth to be 10 kHz. However, this estimate cannot be readily justified, since direct evaluation of the sensor response was not made in a turbulent flow with a known power spectrum.

The objectives of the present study are to develop prototypes of arrayed micro hot-film sensors, which can measure spanwise distributions of the wall shear stress fluctuation, and to evaluate their performance in a wind tunnel. Moreover, a numerical analysis of the unsteady thermal field is made in order to optimize various design parameters of the hot-film shear stress sensor.

ARRAYED MICRO HOT-FILM SENSORS AND EXPERIMENTAL CONDITION

Figure 1(a) shows a schematic of the micro hot-film shear stress sensor developed in the present study. A platinum thin-film heater is deposited on a Si_3N_4 diaphragm of 1μm in thickness. In order to keep the electric resistance of the heater large enough, thin line of platinum is patterned zigzag in an area of 200×23 μm^2. An air cavity of 200 μm in depth is formed underneath the diaphragm by anisotropic etching of the silicon substrate. Another platinum resistor is deposited on the substrate for temperature compensation. For Type 1 sensor, the length of the heater is 200 μm, and the diaphragm is 400×400 μm^2 (Fig. 1b). Eight sensors are fabricated on one chip with 1 mm spacing, and an array of 48 sensors was made by attaching 6 sensor chips onto a print circuit board, which has electric connections to external circuits (Fig. 1d).

Type 2 sensor is designed for the simultaneous measurement of the streamwise and spanwise wall shear stress components, because the spanwise wall shear

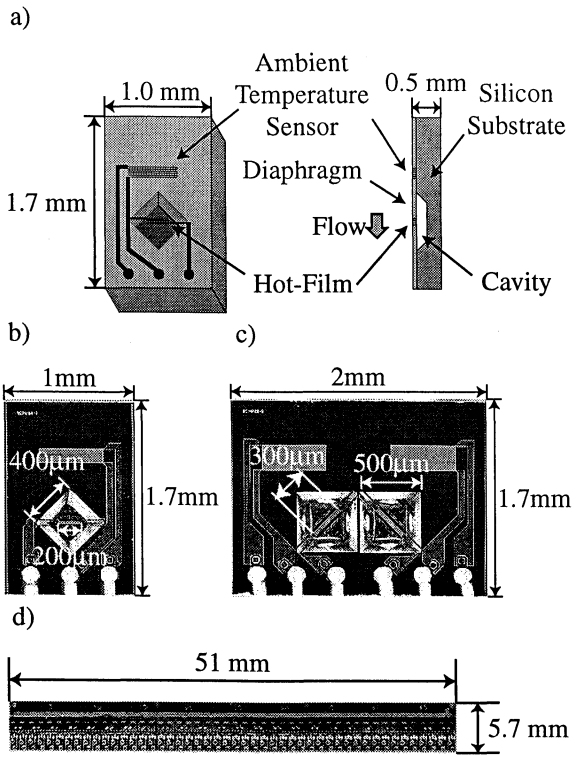

Figure 1 Arrayed micro hot-film shear stress sensors. a) Schematic of Type 1, b) Magnified view of Type 1, c) Magnified view of Type 2, d) One row of 48 sensors.

stress is useful in detecting the near-wall coherent structures (Lee et al., 1998; Endo et al., 2000). Each sensor has two hot-films (300 × 32 μm^2), which are perpendicular to each other (Fig. 1c). The dimensions of the diaphragms are 500 × 500 μm^2. The spacing between the center of the hot-films is 530 μm, while the spanwise spacing between neighboring sensors is 2 mm. It is noted that the physical property of the materials employed in the present sensors is similar to those of Jiang et al. (1996), who designed a 2 μm-thick vacuum cavity under the diaphragm.

Each sensor is driven as a constant temperature anemometer and kept at about 60 °C higher than the ambient temperature. Measurements were made in a fully-developed turbulent air channel flow of a cross section of 50 × 500 mm^2. The bulk mean velocity U_m is changed from 2.5 to 9.3 m/s, which corresponds to the Reynolds number Re_τ based on the wall friction velocity u_τ and the channel half-width from 250 to 800. The reciprocal of the Kolmogorov's time scale for Re_τ = 300 and 670 is respectively about 1000 Hz and 5600 Hz. The streamwise wall pressure gradient was employed to determine the mean wall shear stress. The output voltage of the bridge circuit is digitized with a 16 bit A/D converter at 10 kHz.

A third-order polynomial of the bridge voltage squared was used as a fitting function for the sensor calibration. For Type 2, a modified cosine law is assumed for the dependence of the effective cooling velocity τ_{eff} on the tangential wall shear stress component. Thus, τ_{eff} is given by

$$\tau_{eff} = |\tau|\sqrt{\cos^2\theta + k^2\sin^2\theta}. \quad (1)$$

where θ is the angle between the direction normal to the hot-film and the shear stress vector, τ. The constant k is determined by a least-square method of the calibration data obtained at several velocities and attack angles of the sensor to the streamwise direction. The sensitivity of the present sensor to the tangential wall shear stress is larger than that of the conventional hot-film, and the resultant value of k is 0.6-0.7.

Suzuki & Kasagi (1992) show that the spanwise velocity fluctuation near the wall is significantly overestimated by V-shaped hot-film probes. They have found that the spanwise velocity measured suffers from the substantial difference in the streamwise velocities at two hot-film locations displaced in the spanwise direction. According to their analytical formula of estimating the error, the rms value of the spanwise wall shear stress would be overestimated by 40 and 130 % at Re_τ = 300 and 600, respectively.

STATISTICS OF WALL SHEAR STRESSES

Figure 2 shows the rms streamwise and spanwise wall shear stresses $\tau_{u\,rms}$ and $\tau_{w\,rms}$ normalized by the mean streamwise shear stress $\tau_{u\,mean}$. Kim et al. (1987) and Alfredsson et al. (1988) separately showed that these quantities are independent from the Reynolds number and equal to about 0.4 and 0.2, respectively. For Type 1, the measurement data of $\tau_{u\,rms}$ is in good agreement with the DNS data at Re_τ < 300, but decreases as increasing the Reynolds number because of the imperfect frequency response of the sensor. For Type 2, $\tau_{u\,rms}$ exhibits the similar trend.

On the other hand, the spanwise component $\tau_{w\,rms}$ is almost unchanged. This fact can be explained as follows. As the Reynolds number is increased, the spanwise component would also be decreased. However, because of the increase in the spanwise spacing in wall units between the hot-films, the rms values should be overestimated as mentioned above. Thus,

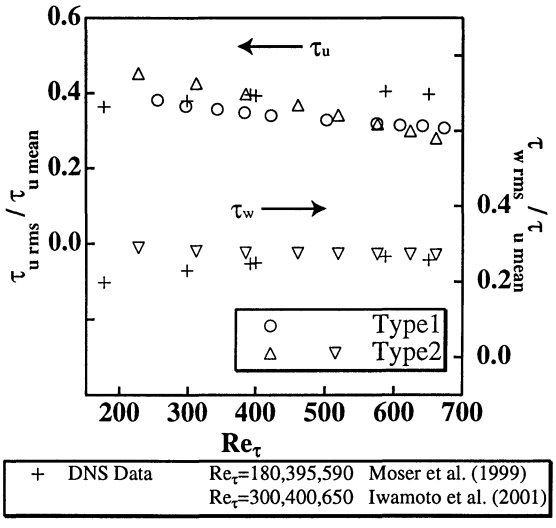

Figure 2 Rms values of wall shear stress fluctuations.

these inverse effects cancel out, and $\tau_{w\,rms}$ remains almost unchanged.

The spanwise two-point correlations of τ_u and τ_w obtained with the arrayed sensors (Fig. 1d) are shown in Fig. 3. The present data are in fairly good accordance with the DNS data. Thus, the near-wall coherent structures, which are the target for feedback control, can be captured with the present wall shear stress

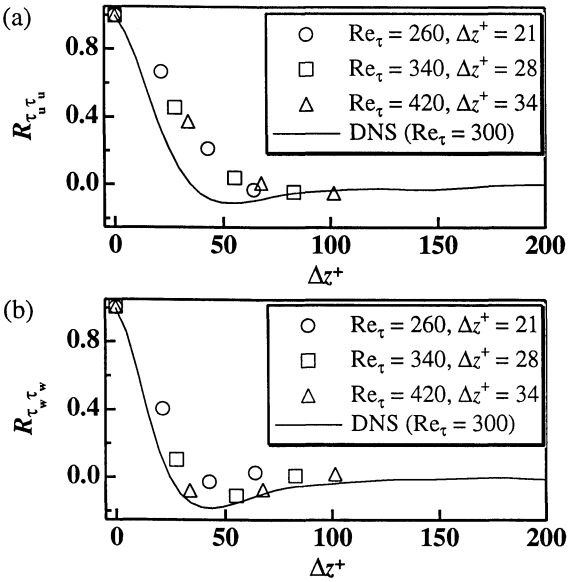

Figure 3 Spanwise two-point correlations.
a) Streamwise shear stress, b) Spanwise shear stress.

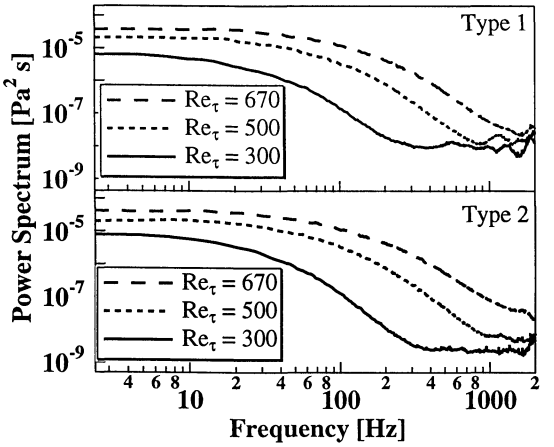

Figure 4 Power spectrum of wall shear stress.

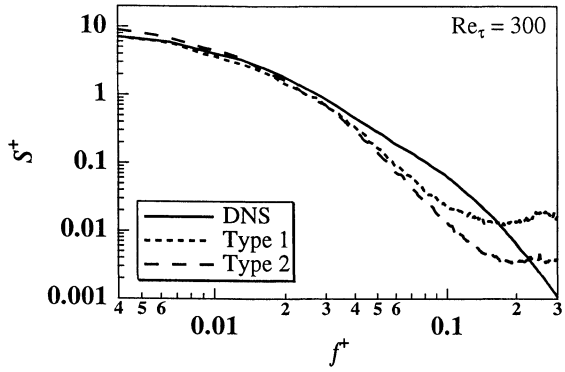

Figure 5 Comparison of power spectrum of the wall shear stress with DNS at Re_τ = 300.

sensors.

Figure 4 shows the power spectra of the streamwise wall shear stress obtained. In this particular measurement, the sensor chip of Type 2 is mounted in such a way that one of the hot-films is perpendicular to the streamwise direction. As expected, the power spectra in the higher frequency range are increased with increasing the Reynolds number. The power spectra for both sensors are in agreement with each other except the spectra in the high frequency range.

Figure 5 shows the power spectra at Re_τ = 300 together with the DNS data of Iwamoto et al. (2001) at the same Reynolds number. The frequency is nondimensionalized with the viscous time unit. The power spectra presently obtained are in good agreement with the DNS data at $f^+ < 0.02$ (f = 40 Hz), but they are clearly decreased at higher frequencies. Therefore, the frequency response of Type 1 and Type 2 sensors is flat up to only 40 Hz at this Reynolds number.

NUMERICAL ANALYSIS OF HOT-FILM SENSORS

It is now clear that the frequency response of the present sensor is much lower than the estimates Jiang et al. (1996) reported. In order to elucidate the cause for this and to design sensors having a wider bandwidth, a numerical analysis of conjugate heat transfer is made.

Numerical Method

A schematic diagram of the computational domain and the boundary conditions are shown in Fig. 6. A two-dimensional model is examined in the present study. Assuming that the dynamic response of the constant temperature bridge circuit is perfect, the temperature of the heater is kept constant. The fluid velocity was given as a linear function of the distance from the wall in order to mimic the fluctuating velocity in the viscous sublayer as follows:

$$u = a(1 + 0.4\sin 2\pi ft)y. \qquad (2)$$

The frequency f is varied from 0 to 2000 Hz. Since the velocity profile is given, the governing energy equation is,

$$\rho C\left(\frac{\partial T}{\partial t} + u\frac{\partial T}{\partial x}\right) = \frac{\partial}{\partial x}\left(\lambda\frac{\partial T}{\partial x}\right) + \frac{\partial}{\partial y}\left(\lambda\frac{\partial T}{\partial y}\right), \qquad (3)$$

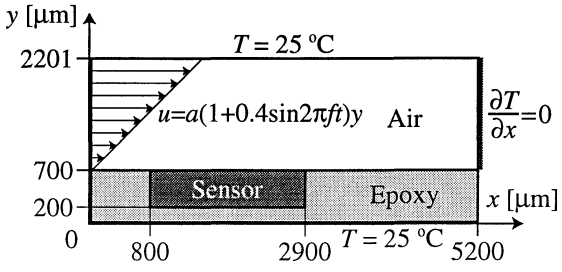

Figure 6 Computational domain and boundary conditions.

where ρ, C and λ are the density, specific heat and thermal conductivity, respectively. A control volume method (Patankar, 1980) is employed for the spatial discretization. A fully-implicit method was used for the temporal discretization.

In the present study, five sensor models listed in Table. 1 are examined. Figure 7 shows a sensor model of Case 3, which is a simplified 2-D model of Type 2. The air cavity is 700μm long and 200 μm deep. On the diaphragm, there are two slits beside the hot-film. Cases 1, 2, and 4 have the same configuration, but has a different length of the cavity. Case 0 is a model of the conventional sensor, in which the hot-film is directly attached to the substrate.

The heat balance near the hot-film is schematically shown in Fig. 8. The heat generated at the hot-film Q_{total} is decomposed into (Q_1+Q_2), where Q_1 denotes the heat transferred to the fluid directly from the hot-film, while Q_2 represents the heat flow conducted to the diaphragm. The heat flow of Q_2 is further divided into Q_3, Q_4, and Q_5 as shown in Fig. 8.

Table. 1 Parameters of sensor models.

	Air Cavity	Air Slit
Case 0	no	no
Case 1	L = 700 μm	no
Case 2	L = 50 μm	no
Case 3	L = 700 μm	yes
Case 4	L = 300 μm	no

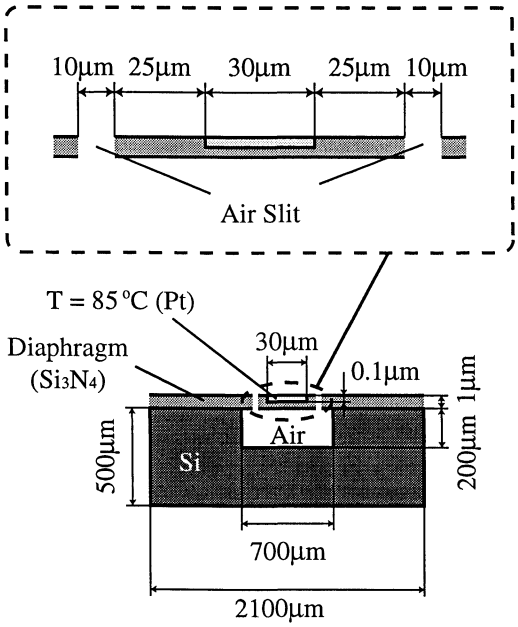

Figure 7 Schematic of sensor model (Case 3).

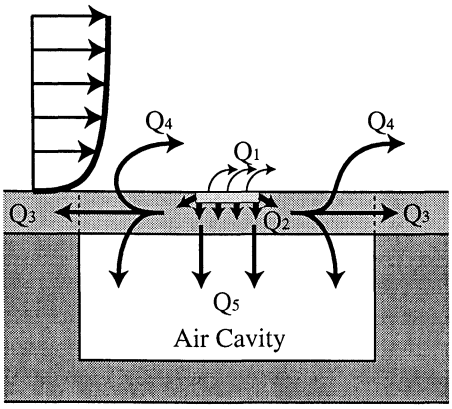

Figure 8 Heat balance near the hot-film.

Evaluation of Heat Balance in Steady State

Figure 9 shows the total heat flow in Case 3 in comparison with the measurement by Type 2, where Q_{total0} is the total heat release in stationary ambient air. Variation of the total heat in Case 3 is in good agreement with that of Type 2, so the present 2-D model can mimic the thermal response of the sensor property.

The contours of temperature and the heat balance at τ_w = 0.04 Pa (Re_τ = 300) are shown in Figs. 10 and 11, respectively. For the conventional sensor (Case 0), contours spread widely in all directions, and the heat loss to the substrate is about 98 % of the total heat generated in the hot-film. Among the heat loss, the heat conduction to the substrate (Q_5) is the largest. On the other hand, for Case 1, which has an insulating air cavity, the heat loss is decreased by 50 %, and the temperature distribution is concentrated close to the diaphragm and in the air cavity. For the sensor with air slits (Case 3), the thermal boundary layer is further reduced due to the reduction of heat conduction in the diaphragm. However, Q_1 is only 12 % of Q_{total} even in Case 3.

It is found that the convective heat transfer from the diaphragm (Q_4) is much larger than Q_1. Moreover, the dependence of Q_4 on τ_w is an order of magnitude larger than that of Q_1. In Case 3, Q_4 is reduced by the air slits, but its variation is still 4 times larger than that of Q_1 (not shown here). When Q_4 is large, the frequency response of the sensor should be deteriorated due to the thermal inertia of the diaphragm. Moreover, the effective sensing area should be enlarged. Therefore, the hot-film shear stress sensor suffers from Q_4, which is considered as the heat transferred from an extended surface.

Frequency Response of Sensor Models

Frequency response of the sensor models are shown

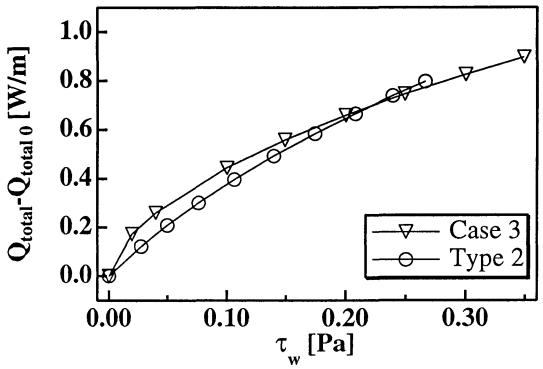

Figure 9 Total heat versus the wall shear stress.

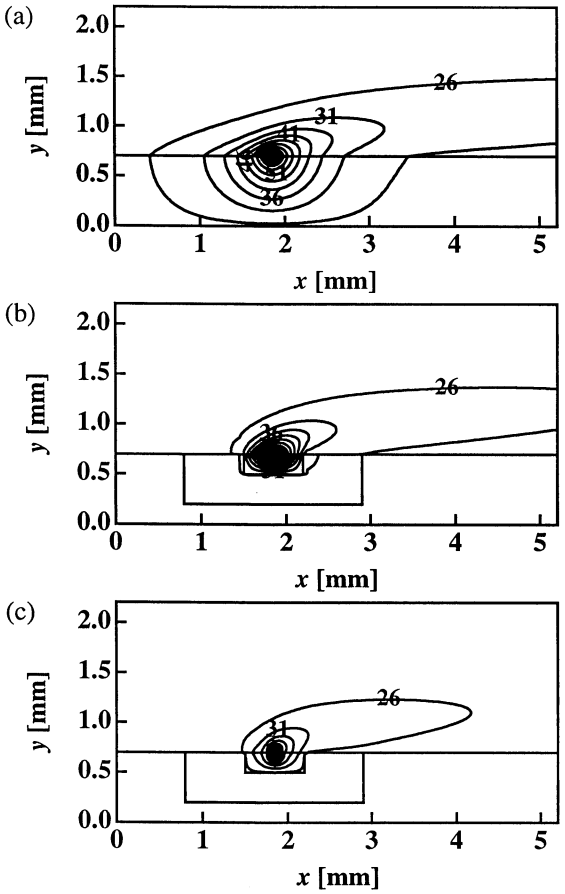

Figure 10 Temperature distribution. a) Conventional sensor (Case 0), b) Sensor with an insulation air cavity (Case 1), c) Sensor with air slits (Case 3).

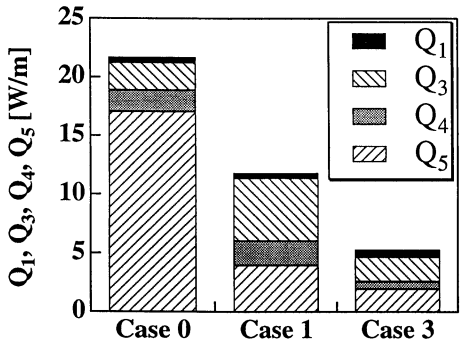

Figure 11 Heat balance at τ_w = 0.04 Pa (Re_τ = 300).

in Fig. 12. It is found that the response is rapidly deteriorated with increasing the frequency and the gain is 0.2 - 0.7 at 200 Hz. The sensors with an air cavity except Case 2 have better response than Case 0. Case 4, which has a cavity shorter than that of Case 1, exhibits better frequency response due to the reduction of Q_4. However, if the length of cavity is further decreased (Case 2), the frequency response is dropped. This is because the thermal crosstalk with the substrate is increased when the length is short. Therefore, once the material and thickness of the diaphragm is given, an optimum length of the cavity should be determined. Reduction of Q_4 with air slits also contributes to the

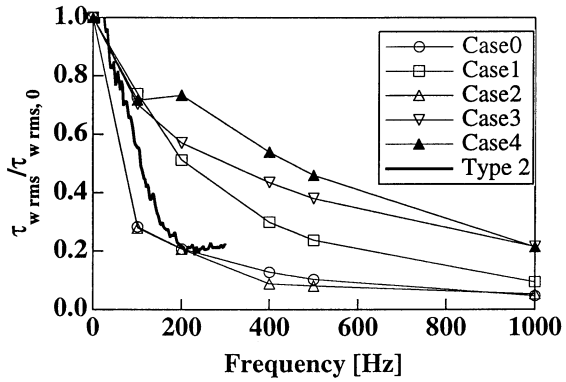

Figure 12 Frequency response of the sensor models.

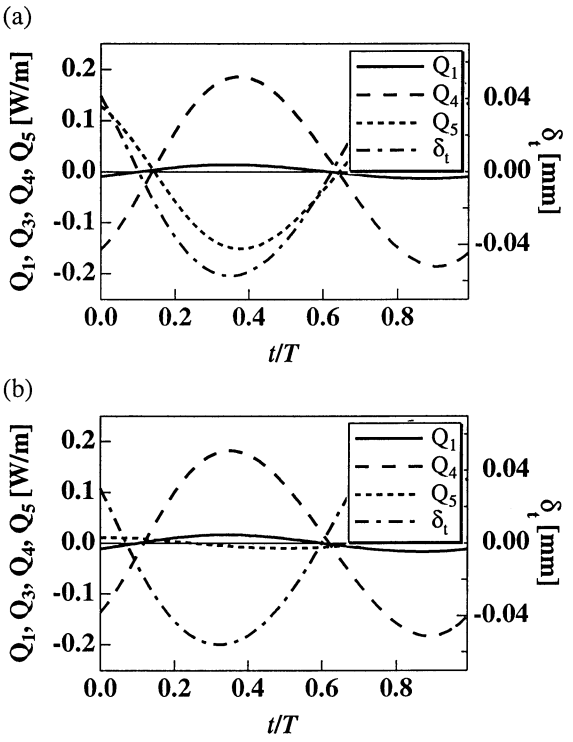

Figure 13 Variation of a heat transfer rate and a thermal boundary layer thickness during the oscillation cycle for the wall shear stress (200 Hz). a) Case 0, b) Case 1.

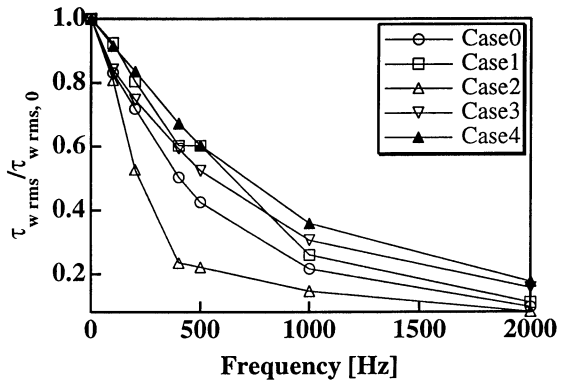

Figure 14 Frequency response based on Q_1.

improvement of the bandwidth in Case 3.

The present sensor Type 2 shows a similar trend, but its gain is smaller than its computational model Case 3. Further analysis should be required to clarify the cause of the difference in frequency response.

Figure 13 shows the temporal variation of the heat flows of Q_1, Q_3, Q_4, and Q_5 together with the thickness of the thermal boundary layer above the hot-film at f = 200 Hz. For Case 1, the amplitude of Q_4 is much larger than that of Q_1, and Q_4 has a large contribution to the total heat loss Q_2. Note that the amplitude of Q_5 is small, so that the frequency response is not affected by the heat loss to the air cavity. Although it is not shown here, the bandwidth is not improved even if a vacuum cavity is assumed. It is also noted that the time delay of Q_1 and Q_4 against the oscillating shear stress is almost the same as that of the thermal boundary layer thickness δt. Therefore, the response of the thermal field near the hot-film is also the source of the poor response of the sensor. For Case 3, the amplitude of Q_4 is decreased by 50 %, which contributes to the improvement of the frequency response. However, the delay of δ_t is almost unchanged (not shown here).

Figure 14 shows the frequency response when the wall shear stress is assumed to be measured by only using Q_1. This is not the case in real experiments, but it clarifies the effect of the thermal boundary layer on the response. The frequency response of the sensors is much improved, but the gain is still insufficient for high frequencies. Therefore, not only the heat conduction in the sensor chip, but also the thermal field above the hot-film is the source of imperfect response of the sensor.

CONCLUSIONS

Prototypes of arrayed micro hot-film sensors were developed and their performance was evaluated in a turbulent channel flow. The rms streamwise wall shear stress fluctuation was in good agreement with the DNS data at low Reynolds numbers, but decreased as increasing the Reynolds number because of the imperfect response of the sensor. Direct evaluation of the frequency response was made in a turbulent flow with a known power spectrum. It was found that the frequency response should be much lower than previous estimates.

A numerical analysis of the thermal field reveals that the frequency response of the sensor is deteriorated by the large by-pass heat transfer from the diaphragm and the phase delay of the thermal boundary layer in the sublayer. According to these results, the dimensions of air cavity can be optimized, once the material and thickness of the diaphragm are prescribed.

ACKNOWLEDGMENTS

The authors thank Mr. M. Murakami for his assistance in the laboratory work. This work was partially supported through the Project for Organized Research Combination System, and also through the Grant-in-Aid for Science Research on Priority Areas (B) by the Ministry of Education, Culture, Sports, Science and Technology of Japan (MEXT).

REFERENCES

Alfredsson, P. H., Johansson, A. V., Haritonidis, J. H., and Eckelmann, H., 1988, "The fluctuating wall-shear stress and the velocity field in the viscous sublayer", Physics of Fluids, 31, pp. 1026-1033.

Endo, T., Kasagi, N., and Suzuki, Y., 2000, "Feedback control of wall turbulence with wall deformation", Int. J. Heat & Fluid Flow, 21, pp. 568-575.

Gad-el-Hak, M., 1996, "Modern developments in flow control", Appl. Mech. Rev., 49, pp. 365-379.

Ho, C. M., and Tai, Y. C., 1998, "Micro-electro-mechanical-systems (MEMS) and fluid flows," Annu. Rev. Fluid Mech., 30, pp. 579-612.

Iwamoto, K., Suzuki, Y., and Kasagi, N., 2001, "Effect of nonlinear interaction on feedback control of wall turbulence," 2nd Int. Symp. Turbulence and Shear Flow Phenomena, Stockholm, to be presented.

Jiang, F., Tai, Y. C., Gupta, B., Goodman, R., Tung, S., Huang, J. B., and Ho, C. M., 1996, "A surface-micromachined shear stress imager," Proc. IEEE Workshop on MEMS, pp. 110-115.

Kasagi, N., 1998, "Progress in direct numerical simulation of turbulent transport and its control," Int. J. Heat & Fluid Flow, 19, pp. 125-134.

Kim, J., Moin, P., and Moser, R., 1987, "Turbulence statistics in fully developed channel flow at low Reynolds number," J. Fluid Mech., 177, pp. 133-166.

Lee, C., Kim, J., and Choi, H., 1998, "Suboptimal control of turbulent channel flow for drag reduction," J. Fluid Mech., 358, pp. 245-258.

Mitchell, J. E., and Hanratty, T. J., 1966, "A study of turbulence at a wall using an electrochemical wall shear-stress meter," J. Fluid Mech., 26, pp. 199-221.

Moin, P., and Bewley, T., 1994, "Feedback control of turbulence," Appl. Mech. Rev., 47, pp. S3-S13.

Moser, R. D., Kim, J., and Mansour, N. N., 1999, "Direct numerical simulation of turbulent channel flow up to Re_τ=590," Phys. Fluids, 11, pp. 943-945.

Naqwi, A. A., and Reynolds, W. C., 1991, "Measurement of turbulent wall velocity gradients using cylindrical waves of laser light," Exp. Fluids, 10, pp. 257-266.

Obi, S., Inoue, K., Furukawa, T., and Maeda, S., 1996, "Experimental study on the statistics of wall shear stress in turbulence channel flow," Int. J. Heat & Fluid Flow, 17, pp. 187-192.

Patanker, S. V., 1980, "Numerical heat transfer and fluid flow," Hemisphere.

Schmidt, M. A., Howe, R. T., Senturia, S. D., and Haritonidis, J. H., 1988, "Design and calibration of a microfabricated floating element shear-stress sensor," IEEE Trans. Electron Device, 35, pp. 750-757.

Suzuki, Y., and Kasagi, N., 1992, "Evaluation of hot-wire measurements in wall shear turbulence using a direct numerical simulation database," Exp. Therm. Fluid Sci., 5, pp. 69-77.